Nonequilibrium phases and phase transitions of the XY model

Tharnier O. Puel [1,2,*] Stefano Chesi [3,4,†] Stefan Kirchner,[1,2,‡] and Pedro Ribeiro[5,3,§]

[1]*Zhejiang Institute of Modern Physics and Department of Physics, Zhejiang University, Hangzhou, Zhejiang 310027, China*

[2]*Zhejiang Province Key Laboratory of Quantum Technology and Device, Zhejiang University, Hangzhou 310027, China*

[3]*Beijing Computational Science Research Center, Beijing 100193, China*

[4]*Department of Physics, Beijing Normal University, Beijing 100875, China*

[5]*CeFEMA, Instituto Superior Técnico, Universidade de Lisboa, Avenida Rovisco Pais, 1049-001 Lisboa, Portugal*

(Received 22 September 2020; accepted 10 December 2020; published 7 January 2021)

We obtain the steady-state phase diagram of a transverse-field XY spin chain coupled at its ends to magnetic reservoirs held at different magnetic potentials. In the long-time limit, the magnetization bias across the system generates a current-carrying nonequilibrium steady state. We characterize the different nonequilibrium phases as functions of the chain's parameters and magnetic potentials, in terms of their correlation functions and entanglement content. The mixed-order transition, previously observed for the case of a transverse-field Ising chain, is established to emerge as a generic feature of a wider class of out-of-equilibrium problems. The critical exponents associated with this universality class are determined analytically. Results are also contrasted with those obtained in the limit of Markovian reservoirs. Our findings should prove helpful in establishing the properties of nonequilibrium phases and phase transitions of extended open quantum systems.

DOI: 10.1103/PhysRevB.103.035108

I. INTRODUCTION

Quantum matter out of thermal equilibrium has become a central research topic in recent years. An important class of problems deal with nonequilibrium quantum states of systems that are in contact with multiple baths, which in turn are held at specified thermodynamic potentials. Such states are not bounded by equilibrium fluctuation relations and thus may host phases of matter that are impossible to realize in equilibrium. Therefore, phase changes far from equilibrium may exist that lack equilibrium counterparts.

Far-from-equilibrium quantum states are routinely realized in mesoscopic solid-state devices [1–3] and recently have also become available in cold atomic gas settings [4]. Thus it is timely to explore the properties of phases of current-carrying matter and address the conditions which have to be met for their emergence.

Nonequilibrium transport across quantum materials dates back to Landauer and Büttiker [5], who were motivated by the failure of semiclassical Boltzmann-like approaches to understand phenomena such as the conductance quantization across mesoscopic conductors. For noninteracting systems, quantum transport is, by now, well understood [6–8]. However, in systems where the physical properties are determined by the electron-electron interaction, progress has been much slower. Here, one often has to resort to either approximate methods or numerically exact techniques [9] which, however, are often restricted to small systems or comparatively high temperatures. Exact analytical results, available for integrable models in one dimension, do not typically generalize to open setups. Moreover, nonthermal steady states in Luttinger liquids [10–12] seem to be less general than their equilibrium counterparts.

Considerable progress has been made in the Markovian case, where the environment lacks memory [13–16]. The applicability of the Markovian case is, however, limited to extreme nonequilibrium conditions (e.g., very large bias or temperature) and is of restricted use for realistic transport setups [17,18].

Other recent developments to study transport include the study of so-called generalized hydrodynamic methods available for integrable systems [19,20] and hybrid approaches involving Lindblad dynamics [21]. However, these methods are not yet able to describe current-carrying steady states in extended mesoscopic systems.

Our recent analysis of the exactly solvable transverse-field Ising chain attached to macroscopic reservoirs has allowed us to study a symmetry-breaking quantum phase transition in the steady state of an extended nonequilibrium system [22]. At the equilibrium level, this model can be mapped onto that of noninteracting fermions via a Jordan-Wigner transformation and is thus solvable by elementary means.

The nonthermal steady state of this model is, however, much richer and allows for a peculiar symmetry-breaking quantum phase transition. In particular, we have shown this transition to be of a mixed-order (or hybrid) nature, with a discontinuous order parameter and diverging correlation length. These types of transitions were first discussed by Thouless in 1969 [23] in the context of classical spin chains with

*tharnier@me.com
†stefano.chesi@csrc.ac.cn
‡stefan.kirchner@correlated-matter.com
§pedrojgribeiro@tecnico.ulisboa.pt

long-range interactions and have since then been reported in different environments [24–28].

Even though realistic systems are only approximately described by exactly solvable models at best, exact solutions are still of considerable value. Not only can they be important in unveiling features of novel effects, but they are commonly instrumental in benchmarking numerical and approximate methods. Therefore, exact solutions are particularly helpful in situations where no reliable numerical or approximate methods yet exist, such as in the description of current-carrying steady states of interacting systems.

In this article, we provide a set of exact results of steady-state phases and phase transitions of an XY spin chain in a transverse field coupled to magnetic reservoirs held at different magnetizations. Our analysis extends and generalizes the findings in Ref. [22] and points out regimes that are not present in the Ising case. In the Markovian limit, we recover previous results obtained for XY spin chains coupled to free-of-memory reservoirs [13,29,30], where an out-of-equilibrium phase transition with spontaneous emergence of long-range order has been found.

The paper is organized as follows. In Sec. II, we define the out-of-equilibrium model and briefly describe the methods used to solve it. In Sec. III, we describe in detail the nonequilibrium phase diagram based on the energy current and the properties of the occupation number. The correlation functions in the various phases are analysed in Sec. IV, where we also discuss the critical behavior at the mixed-order phase transition and the characteristic oscillations in the z-correlation function. Universal features of the entropy and mutual information are discussed in Sec. V. Finally, we summarize and conclude our work in Sec. VI.

II. MODEL AND METHOD

A. Hamiltonian and Jordan-Wigner mapping

We consider an XY-spin chain of N sites (labeled by r), exchange coupling J, and coupled to a transverse field h. At its ends, i.e., at $r = 1$ and $r = N$, the chain is coupled to magnetic reservoirs which are kept at zero temperature ($T = 0$). The Hamiltonian of the chain is given by

$$\mathcal{H}_{\rm C} = -\frac{J}{2}\sum_{r=1}^{N-1}\left[(1+\gamma)\sigma_r^x\sigma_{r+1}^x + (1-\gamma)\sigma_r^y\sigma_{r+1}^y\right] - h\sum_{r=1}^{N}\sigma_r^z, \tag{1}$$

where $\sigma_r^{x,y,z}$ are the Pauli matrices at site r, and γ controls the anisotropy. The total Hamiltonian is given by

$$\mathcal{H} = \mathcal{H}_{\rm C} + \sum_{l={\rm L,R}}(\mathcal{H}_l + \mathcal{H}_{{\rm C}\text{-}l}), \tag{2}$$

where $\mathcal{H}_l$ and $\mathcal{H}_{{\rm C}\text{-}l}$, with $l = $ L,R, are, respectively, the Hamiltonians of the reservoirs and the system-reservoir coupling terms. In the following, we assume that the reservoirs possess bandwidths which are entirely determined by magnetic potential μ_l ($l = L, R$) and which are much larger than the energy scales that characterize the chain.

In the wide-band limit, the results become independent of the details of $\mathcal{H}_l$ and $\mathcal{H}_{{\rm C}\text{-}l}$. For concreteness, we take the reservoirs to be isotropic XY chains, i.e.,

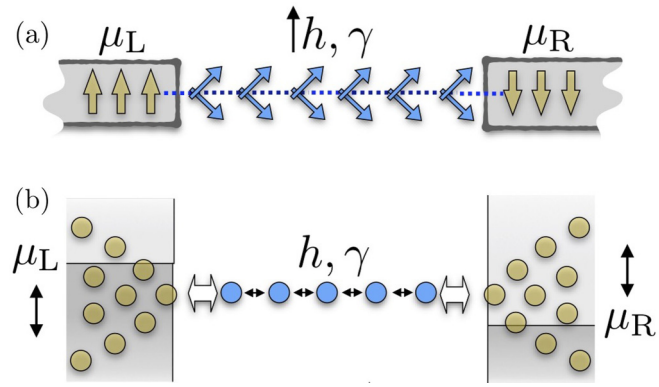

FIG. 1. (a) Schematic picture of the XY-model spin chain in contact with magnetic reservoirs and (b) the same system mapped to its fermionic representation, i.e., a triplet superconducting chain of spinless fermions in contact with fermionic reservoirs.

$$\mathcal{H}_l = -J_l\sum_{r_l\in\Omega_l}\left(\sigma_{r_l}^x\sigma_{r_l+1}^x + \sigma_{r_l}^y\sigma_{r_l+1}^y\right), \tag{3}$$

with $l = L, R$, and we have defined $\Omega_{\rm L} \equiv \{-\infty, \ldots, 0\}$, $\Omega_{\rm R} \equiv \{N+1, \ldots, \infty\}$. Initially, the reservoirs are in an equilibrium Gibbs state, $\rho_l = e^{-\beta(\mathcal{H}_l - \mu_l M_l)}$, where $M_l = \sum_{r_l\in\Omega_l}\sigma_{r_l}^z$ is the reservoir magnetization (which is a good quantum number in the absence of system-reservoir coupling, i.e., $[\mathcal{H}_l, M_l] = 0$). The average value of M_l is set by the magnetic potential μ_l. For finite μ_l, these are non-Markovian reservoirs, with power-law decaying correlations, and a set of gapless magnetic excitations within an energy bandwidth $J_l \gg J, h$. The chain-reservoir coupling Hamiltonians are

$$\mathcal{H}_{{\rm C}\text{-}l} = -J_{{\rm C}\text{-}l}\left(\sigma_{(r_l)_{\rm C}}^x\sigma_{(r)_l}^x + \sigma_{(r)_l}^y\sigma_{(r_l)_{\rm C}}^y\right), \tag{4}$$

with $(r_{\rm L})_{\rm C} = 1$, $(r)_{\rm L} = 0$, $(r_{\rm R})_{\rm C} = N$, and $(r)_{\rm R} = N+1$. A sketch of this system is shown in Fig. 1(a).

The full Hamiltonian $\mathcal{H}$ can be represented in terms of fermions via the so-called Jordan-Wigner (JW) mapping [31], $\sigma_r^+ = e^{i\pi\sum_{r'=1}^{r-1}\hat{c}_{r'}^\dagger\hat{c}_{r'}}c_r^\dagger$, where $\hat{c}_r^\dagger/\hat{c}_r$ creates/annihilates a spinless fermion at site r. The JW-transformed system corresponds to a Kitaev chain [32] in contact with two metallic reservoirs of spinless fermions at chemical potentials $\mu_{\rm L,R}$, i.e.,

$$\mathcal{H} = -J\sum_{r=1}^{N-1}(\hat{c}_r^\dagger\hat{c}_{r+1} + \gamma\hat{c}_r^\dagger\hat{c}_{r+1}^\dagger + {\rm H.c.}) - 2h\sum_{r=1}^{N}\hat{c}_r^\dagger\hat{c}_r - \sum_{l={\rm L,R}}\left[J_{{\rm C}\text{-}l}\hat{c}_{(r_l)_{\rm C}}^\dagger\hat{c}_{(r)_l} + J_l\sum_{r_l\in\Omega_l}\hat{c}_{r_l}^\dagger\hat{c}_{r_l+1} + {\rm H.c.}\right], \tag{5}$$

where $J\gamma$ defines the superconducting coupling strength and h plays the role of a potential applied on the chain. A sketch of this system is shown in Fig. 1(b). In equilibrium, topologically nontrivial phases of the Kitaev chain correspond to magnetically ordered phases of the original XY-spin model, whereas the topologically trivial cases correspond to disordered phases. With a magnetic bias, the transfer of spin excitations between the reservoirs was studied rather extensively (see, e.g., Refs. [33,34]), also considering transport signatures of the topological phase in short junctions [35,36].

Here, however, we will be mostly concerned with the bulk properties at $N \to \infty$, and after the reservoirs have been traced out.

B. Nonequilibrium Green's functions

As the JW-transformed Hamiltonian is quadratic in its fermionic degrees of freedom, the nonequilibrium system admits an exact solution in terms of single-particle quantities. In the following, we employ the nonequilibrium Green's function formalism to compute correlation functions and related observables. The procedure is described in the Supplemental Material of Ref. [22] and is briefly summarized here for convenience.

We start by defining the Nambu vector, $\hat{\boldsymbol{\Psi}}^\dagger = (\hat{c}_1^\dagger, \ldots, \hat{c}_N^\dagger, \hat{c}_1, \ldots, \hat{c}_N)$, and the retarded, advanced, and Keldysh components of the Green's function, given by

$$\boldsymbol{G}^R_{i,j}(t-t') = -i\Theta(t-t')\langle\{\hat{\boldsymbol{\Psi}}_i(t), \hat{\boldsymbol{\Psi}}^\dagger_j(t')\}\rangle, \tag{6}$$

$$\boldsymbol{G}^A_{i,j}(t-t') = i\Theta(t'-t)\langle\{\hat{\boldsymbol{\Psi}}_i(t), \hat{\boldsymbol{\Psi}}^\dagger_j(t')\}\rangle, \tag{7}$$

$$\boldsymbol{G}^K_{i,j}(t-t') = -i\langle[\hat{\boldsymbol{\Psi}}_i(t), \hat{\boldsymbol{\Psi}}^\dagger_j(t')]\rangle. \tag{8}$$

Using this notation, the Hamiltonians for the right and left reservoirs and for the chain are given by $\mathcal{H}_l = \frac{1}{2}\hat{\boldsymbol{\Psi}}^\dagger \boldsymbol{H}_l \hat{\boldsymbol{\Psi}}$, with $l = L, R, C$. For the chain, $\boldsymbol{H}_\mathrm{C}$ is a $2N \times 2N$ Hermitian matrix respecting particle-hole symmetry, i.e., $\boldsymbol{S}^{-1}\boldsymbol{H}_\mathrm{C}^T\boldsymbol{S} = -\boldsymbol{H}_\mathrm{C}$, where $\boldsymbol{S} = \tau^x \otimes \mathbf{1}_{N\times N}$ and τ^x interchanges particle and hole spaces. Similar definitions apply to the degrees of freedom of the right and left reservoirs. The bare retarded and advanced Green's functions, in the absence of chain-reservoir couplings, are simply given by $\boldsymbol{G}^{R/A}_{l,0}(\omega) = (\omega - \boldsymbol{H}_l \pm i\eta)^{-1}$. Rewriting the chain-reservoir coupling in the same notation, $\mathcal{H}_{\mathrm{C}\text{-}l} = \frac{1}{2}(\hat{\boldsymbol{\Psi}}^\dagger_{(l)}\boldsymbol{T}\hat{\boldsymbol{\Psi}} + \hat{\boldsymbol{\Psi}}^\dagger \boldsymbol{T}^\dagger \hat{\boldsymbol{\Psi}}_{(l)})$. The self-energy of the chain, induced by tracing out the reservoirs, is $\boldsymbol{\Sigma}^{R/A/K} = \sum_{l=\mathrm{L,R}} \boldsymbol{\Sigma}^{R/A/K}_l$, where

$$\boldsymbol{\Sigma}^{R/A}_l(\omega) = \boldsymbol{T}^\dagger \boldsymbol{G}^{R/A}_{l,0}(\omega)\boldsymbol{T}, \tag{9}$$

$$\boldsymbol{\Sigma}^K_l(\omega) = \left[\boldsymbol{\Sigma}^R_l(\omega) - \boldsymbol{\Sigma}^A_l(\omega)\right][1 - 2n_{\mathrm{F},l}(\omega)] \tag{10}$$

are the contributions of reservoir l, which obey equilibrium fluctuation-dissipation relations, and where $n_{\mathrm{F},l}(\omega) = (e^{\beta_l(\omega-\mu_l)} + 1)^{-1}$ is the Fermi function with chemical potential μ_l and inverse temperature β_l. The chain steady-state Green's functions are obtained from the Dyson's equation,

$$\boldsymbol{G}^{R/A}_\mathrm{C}(\omega) = \left[\boldsymbol{G}^{R/A}_{\mathrm{C},0}(\omega) - \boldsymbol{\Sigma}^{R/A}(\omega)\right]^{-1}, \tag{11}$$

$$\boldsymbol{G}^K_\mathrm{C}(\omega) = \boldsymbol{G}^R_\mathrm{C}(\omega)\boldsymbol{\Sigma}^K(\omega)\boldsymbol{G}^A_\mathrm{C}(\omega). \tag{12}$$

As mentioned above, we consider the case where the bandwidths of the reservoirs, $J_{l=\mathrm{L,R}}$, are much larger than the other energy scales. In this wide-band limit, the coupling to reservoir l is completely determined by the hybridization energy scale $\Gamma_l = \pi J^2_{\mathrm{C}\text{-}l} D_l$. Here, D_l is the reservoir's constant-local density of states. In practice, the wide-band limit yields a frequency-independent retarded self-energy, $\boldsymbol{\Sigma}^R_l = i(\boldsymbol{\gamma}_l + \bar{\boldsymbol{\gamma}}_l)$, which substantially simplifies subsequent calculations, with $\boldsymbol{\gamma}_l = \Gamma_l |r_l\rangle\langle r_l|$ and $\bar{\boldsymbol{\gamma}}_l = \Gamma_l |\bar{r}_l\rangle\langle\bar{r}_l|$, and where $|r\rangle$ and $|\bar{r}\rangle \equiv \boldsymbol{S}|r\rangle$ are single-particle and hole states.

In this case, it is convenient to define the non-Hermitian single-particle operator,

$$\boldsymbol{K} \equiv \boldsymbol{H}_\mathrm{C} - i\sum_{l=\mathrm{L,R}} (\boldsymbol{\gamma}_l + \bar{\boldsymbol{\gamma}}_l), \tag{13}$$

which we assume to be diagonalizable, possessing right and left eigenvectors $|\alpha\rangle$ and $\langle\tilde{\alpha}|$, and associated eigenvalues λ_α. In terms of these quantities, the retarded Green's function is given by

$$\boldsymbol{G}^R(\omega) = (\omega - \boldsymbol{K})^{-1} = \sum_\alpha |\alpha\rangle(\omega - \lambda_\alpha)^{-1}\langle\tilde{\alpha}|, \tag{14}$$

and the Keldysh Green's function becomes

$$\boldsymbol{G}^K(\omega) = -2i\sum_l \sum_{\alpha\beta} |\alpha\rangle\langle\beta| \times \frac{\langle\alpha'|\boldsymbol{\gamma}_l|\beta'\rangle[1 - 2n_{\mathrm{F},l}(\omega)] - \langle\alpha'|\bar{\boldsymbol{\gamma}}_l|\beta'\rangle[1 - 2n_{\mathrm{F},l}(-\omega)]}{(\omega - \lambda_\alpha)(\omega - \bar{\lambda}_\beta)}. \tag{15}$$

Steady-state observables can be obtained from the single-particle correlation function matrix, $\boldsymbol{\chi} \equiv \langle\hat{\boldsymbol{\Psi}}\hat{\boldsymbol{\Psi}}^\dagger\rangle$, which is obtained from the Keldysh Green's function,

$$\boldsymbol{\chi} = \frac{1}{2}\left[i\int \frac{d\omega}{2\pi}\boldsymbol{G}^K(\omega) + \mathbf{1}\right]. \tag{16}$$

The explicit form of $\boldsymbol{\chi}$ after performing the integration over frequencies is provided in Eq. (A1). As the model is quadratic, $\boldsymbol{\chi}$ encodes all the information about the reduced density matrix of the chain, $\hat{\rho}_\mathrm{C} = \mathrm{tr}_{\mathrm{L,R}}[\hat{\rho}]$. This quantity can itself be expressed as the exponential of a quadratic operator, i.e., $\hat{\rho}_\mathrm{C} = e^{\hat{\Omega}_\mathrm{C}}/Z$, where $Z = \mathrm{tr}[e^{\hat{\Omega}_\mathrm{C}}]$ and $\hat{\Omega}_\mathrm{C} = \frac{1}{2}\hat{\boldsymbol{\Psi}}^\dagger \boldsymbol{\Omega}_\mathrm{C}\hat{\boldsymbol{\Psi}}$ with $\boldsymbol{\Omega}_\mathrm{C}$ being a $2N \times 2N$ matrix respecting the particle-hole symmetry conditions. $\hat{\Omega}_\mathrm{C}$ is related to the single-particle density matrix via

$$\boldsymbol{\chi} = (e^{\boldsymbol{\Omega}_\mathrm{C}} + \mathbf{1})^{-1}. \tag{17}$$

This relation allows the calculation of mean values of quadratic observables, $\hat{O} = \frac{1}{2}\hat{\boldsymbol{\Psi}}^\dagger \boldsymbol{O}\hat{\boldsymbol{\Psi}}$, defined by the Hermitian and particle-hole symmetric matrix $\boldsymbol{O}$,

$$\langle\hat{O}\rangle = \mathrm{Tr}[\hat{\rho}_\mathrm{C}\hat{O}] = -\tfrac{1}{2}\mathrm{tr}[\boldsymbol{O}\cdot\boldsymbol{\chi}], \tag{18}$$

as well as all higher-order correlation functions.

III. PHASE DIAGRAM

This section discusses the nonequilibrium phase diagram of the model, as well as the excitations and associated occupation numbers in the various different phases. To contextualize our findings, the first two sections are devoted to a brief description of the equilibrium properties of the XY chain and a review of the nonequilibrium Markovian limit.

A. Equilibrium phases

The system in equilibrium is more conveniently studied without considering the couplings to the leads and assuming periodic boundary conditions. After performing the JW transformation, the Hamiltonian of the translation-invariant chain is diagonalized in the momentum representation by a suitable

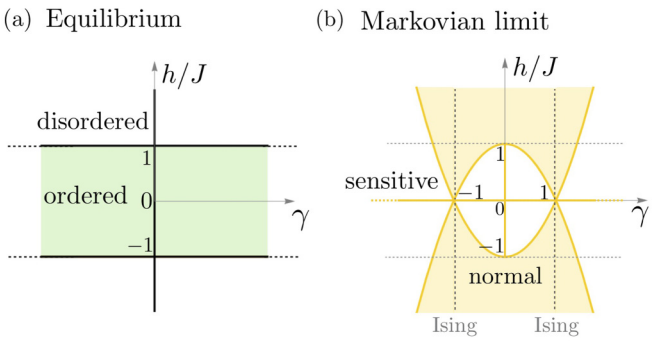

FIG. 2. (a) Phase diagram $h/J \times \gamma$ of the XY model in equilibrium. The black thick lines identify a gap closing. (b) Phase diagram of the out-of-equilibrium XY model according to the presence (sensitive) or absence (normal) of long-range correlations in the Markovian limit. The vertical dashed line at $\gamma = +1$ ($\gamma = -1$) identifies the Ising model with only $XX(YY)$-spin-coupling interactions.

Bogoliubov transformation, i.e., $\mathcal{H}_C = \sum_k \varepsilon_k(\hat{\gamma}_k^\dagger \hat{\gamma}_k - 1/2)$, where the operators $(\hat{\gamma}_k, \hat{\gamma}_{-k}^\dagger)^T = e^{i\theta_k \sigma_x}(\hat{c}_k, \hat{c}_{-k}^\dagger)^T$ describe excitations of energy

$$\varepsilon_k = 2J\sqrt{(h/J + \cos k)^2 + (\gamma \sin k)^2}, \tag{19}$$

and $\sin(2\theta_k) = -2J\gamma \sin(k)/\varepsilon_k$.

The ground state is characterized by a vanishing number of Bogoliubov excitations, i.e., $n_k = 0$, where

$$n_k \equiv \langle \hat{\gamma}_k^\dagger \hat{\gamma}_k \rangle. \tag{20}$$

For $|h/J| < 1$, the ground state is topologically nontrivial with positive and negative anisotropies ($\gamma > 0$ or <0) corresponding to opposite signs of the topological invariant, separated by a critical gapless state for $\gamma = 0$. At $|h/J| = 1$, the spectral gap vanishes and the system transitions into a topologically trivial phase at large h.

A similar phase diagram is obtained in terms of the original spin degrees of freedom. Figure 2(a) illustrates the zero-temperature phase diagram of the equilibrium XY model. For $\gamma > 0$, the system is magnetically ordered along the x direction under a weak transverse field h, and possesses a finite magnetization [37] $\phi \equiv \lim_{h_x \to 0} \lim_{L \to \infty} \frac{1}{N} \sum_r \langle \sigma_r^x \rangle \neq 0$, where h_x is a symmetry-breaking magnetic field along the x direction. A negative anisotropy, i.e., $\gamma < 0$, yields a nonvanishing magnetization along the y direction, whereas at $\gamma = 0$, the system is critical and isotropic for $|h/J| < 1$. As the ordered phases for $\gamma > 0$ and <0 are equivalent to each other and related via a simple rotation, only $\gamma > 0$ is considered in the subsequent analysis. It is worth recalling that the special cases $\gamma = \pm 1$ correspond to the transverse-field Ising model. A strong h drives the magnetic phase through a second-order phase transition into a phase of vanishing magnetization, i.e., a phase with $\phi = 0$. Near the transition, for $|h/J| < 1$, the magnetization behaves as $\phi \simeq \sqrt{\frac{2}{1+|\gamma|}}\{\gamma^2[1 - (h/J)^2]\}^{1/8}$ [37].

The computation of the order parameter, ϕ, directly from the above definition is not possible via the JW mapping. Instead, one considers the two-point correlation functions ($\alpha = x, y, z$),

$$\mathbb{C}_{r,r'}^{\alpha\alpha} = \langle \sigma_r^\alpha \sigma_{r'}^\alpha \rangle - \langle \sigma_r^\alpha \rangle \langle \sigma_{r'}^\alpha \rangle. \tag{21}$$

For disordered phases in equilibrium, these correlators are expected to show either exponential (EXP) or power-law (PL) decay depending on whether the system is gapped or gapless. In the ordered phase, the system has long-range order (LRO) correlations, e.g., for $\gamma > 0$,

$$\mathbb{C}_{r,r'}^{xx} \simeq A e^{-|r-r'|/\xi} + \phi^2, \tag{22}$$

where ξ is the characteristic correlation length and A is a numeric coefficient. This expression allows one to obtain ϕ from the correlation function $\mathbb{C}_{r,r'}^{xx}$, which in turn can be computed in terms of a Toeplitz determinant [31,38]. In equilibrium, all correlation functions, except $\mathbb{C}_{r,r'}^{xx}$, either vanish or decay exponentially with $|r - r'|$.

For an open system connected to demagnetized baths, i.e., $\mu_{L,R} = 0$, the same equilibrium bulk properties as those for the closed system are found. It is natural to expect that bulk properties pertain for distances greater than ξ away from the leads. Our calculation of fermionic observables follows that described in Sec. II. The calculation of the spin-spin correlation functions is similar to those for the translation-invariant system and is given in Appendix A in terms of the single-particle correlation matrix $\boldsymbol{\chi}$.

B. Nonequilibrium phases in the Markovian limit

The nonequilibrium features of the XY model with Markovian reservoirs were first reported in Refs. [13,39]. This limit can be recovered from the present model by taking $|\mu_R|$ or $|\mu_L| \to \infty$ [17]. The steady-state phase diagram in that limit possesses two distinct phases, one characterized by an exponential decay of all correlation functions with distance and the other by an algebraic decay of $\mathbb{C}_{r,r'}^{zz}$, concomitant with a strong sensitivity to small variations of some control parameters [13]. We dub these regimes as normal and sensitive phases, respectively. Figure 2(b) depicts the phase diagram in this Markovian limit and with its sensitive (white) and normal (light-yellow) phases. The dark-yellow lines mark critical phase boundaries.

The quasiparticle dispersion relation, given by Eq. (19), is shown in Figs. 3(a) and 3(c). The algebraic correlations are associated to the presence of an inflection point in the quasiparticle dispersion which appears for $h/J \leqslant |1 - \gamma^2|$. In the normal region, the extrema of the energy are $m_1 = \varepsilon_{k=0} = 2J|1 + h/J|$ and $m_2 = \varepsilon_{k=\pi} = 2J|1 - h/J|$, while for the sensitive region, $m_3 = 2J|\gamma|\sqrt{1 + (h/J)^2(\gamma^2 - 1)^{-1}}$ becomes a global extremum. Figures 3(b) and 3(d) show the spectrum of the non-Hermitian single-particle operator $\boldsymbol{K}$ [see Eq. (13)] for both normal and sensitive phases. It turns out that the imaginary part of the eigenvalues scales with the inverse system size, $\mathrm{Im}\lambda_\alpha \propto N^{-1}$ [40]. This is a reflection of the fact that for the chain degrees of freedom, the dissipative effects of the boundary become less important with increasing system size. A key feature of the sensitive region is that for energies [i.e., $\mathrm{Re}(\lambda_\alpha)$] where four momenta can propagate, the spectrum does not converge to a line with increasing system size, but becomes scattered within a finite area [13]. These effects are independent of the Markovian nature of the reservoirs and remain for the non-Markovian case as the operator $\boldsymbol{K}$ does not depend on the chemical potential of the leads. Thus, as explicitly shown below, the normal-sensitive

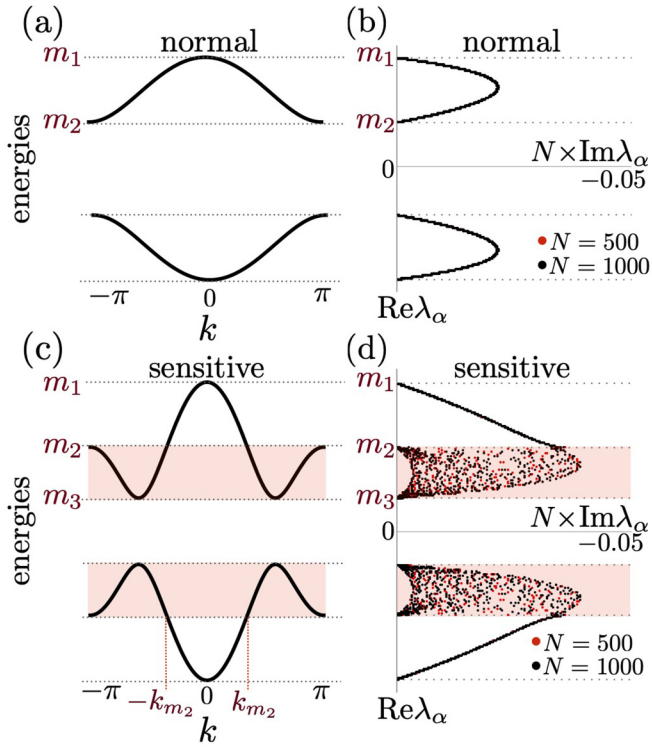

FIG. 3. Quasiparticle dispersion relation of the equilibrium XY model in the (a) normal and (c) sensitive regions, with $\{\gamma, h/J\} = \{1.0, 0.2\}$ and $\{\gamma, h/J\} = \{0.5, 0.2\}$, respectively, which leads to $\{m_1, m_2, m_3\} = \{2.4, 1.6, 0.97\}$. $\pm k_{m_2}$ are the two momenta with energy m_2. (b) and (d) depict the eigenvalues λ_α of the non-Hermitian single-particle operator $\boldsymbol{K}$ in the complex plane.

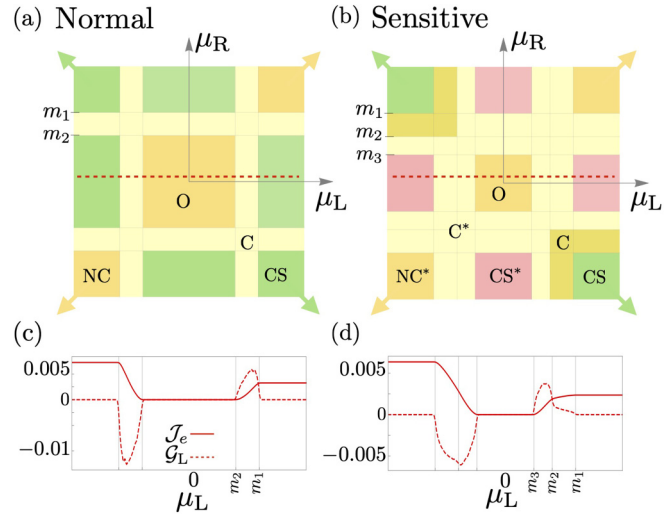

FIG. 4. Non-Markovian phase diagram $\mu_\mathrm{L} \times \mu_\mathrm{R}$ of two illustrative settings inside the (a) normal and (b) sensitive regions, following the same set of parameters in Fig. 3. The phases were defined as ordered (O), conducting (C), conducting saturated (CS), and nonconducting (NC). In the sensitive case, the phases which acquire a noise in the occupation number are signed with a star *. The arrows at the corners indicate the Markovian limit, i.e., $|\mu_\mathrm{R}|$ and $|\mu_\mathrm{L}| \to \pm\infty$. (c) and (d) show the current of energy ($\mathcal{J}_e$) and the conductance ($\mathcal{G}_\mathrm{L} \equiv \partial_{\mu_\mathrm{L}} \mathcal{J}_e$) computed across the red dotted lines drawn on the phase diagrams (a) and (b), respectively.

transition, reported in Refs. [13,39] for the Markovian case, also occurs for finite values of μ_L and μ_R.

C. Nonequilibrium phase diagram: Energy current

We now present the phase diagram of the nonequilibrium XY model and show that the energy current passing through the chain can be used to discriminate between the different phases.

Conservation of energy implies that the steady-state energy current is equal across any cross section along the chain and can be obtained from $\boldsymbol{\chi}$ as

$$\mathcal{J}_e = -\tfrac{1}{2}\,\mathrm{tr}[\boldsymbol{J}_r \cdot \boldsymbol{\chi}], \tag{23}$$

where $\boldsymbol{J}_r$ is the single-particle current operator at link $(r, r+1)$ which is explicitly given in Appendix A.

We have previously discussed the steady-state energy current in a non-Markovian setting for the particular case of the transverse-field Ising model, i.e., $|\gamma| = 1$, in Ref. [22]. The nonequilibrium phase diagram, as a function of μ_L and μ_R, in the normal phase is qualitatively similar to the Ising case and is reproduced in Fig. 4(a). Two of the phases which arise near $\mu_\mathrm{L} = \mu_\mathrm{R}$ do not support energy transport, i.e., $\mathcal{J}_e = 0$: the ordered phase (O) and the nonconducting phases (NC). Other phases may be further characterized in terms of their energy conductance, i.e., $\mathcal{G}_\mathrm{L} \equiv \partial_{\mu_\mathrm{L}} \mathcal{J}_e$ and $\mathcal{G}_\mathrm{R} \equiv \partial_{\mu_\mathrm{R}} \mathcal{J}_e$. The current-saturated (CS) phases are those with $\mathcal{J}_e \neq 0$ and $\mathcal{G}_\mathrm{R} = \mathcal{G}_\mathrm{R} = 0$. They arise when one of the reservoir's chemical potentials is larger than m_1, while the other lies inside the quasiparticle excitation gap. The conducting phase (C) is characterized by a nonzero conductance, i.e., $\mathcal{G}_\mathrm{L} \neq 0$ and/or $\mathcal{G}_\mathrm{R} \neq 0$, arising whenever at least one of the chemical potentials lies within the quasiparticle excitations band, i.e., $|\mu_\mathrm{L}|$ and/or $|\mu_\mathrm{R}| \in (m_1, m_2)$.

Figure 4(b) depicts the phase diagram for a generic XY chain. Besides the phases found for $\gamma = 1$, an analysis of the occupation numbers (see next section) shows that some regions acquire a noiselike behavior. These phases, similar to the sensitive regions of the Markovian case, are labeled NC*, CS*, and C*.

In Figs. 4(c) and 4(d), we show the current $\mathcal{J}_e$ and conductance $\mathcal{G}_\mathrm{L}$ for a fixed μ_R represented by the red dashed lines in the phase diagrams. In the sensitive region, the C phase is crossed by the transition line at $\mu_\mathrm{L} = m_2$, where the conductance becomes nonanalytic. It is worth noting that the noiselike behavior found in the occupation numbers does not appear in the current of energy.

In terms of the JW fermions, the present analysis is similar to that of a transport across a tight-binding model in the sense that when the chemical potentials cross the dispersion relation, nonanalytic properties of the current appear. However, the existence of anomalous terms in the fermionic Hamiltonian inhibits a closer comparison with charge transport.

D. Occupation numbers

In the current-carrying steady-state regime of a Fermi gas, fluctuations in the number of particles were shown to be

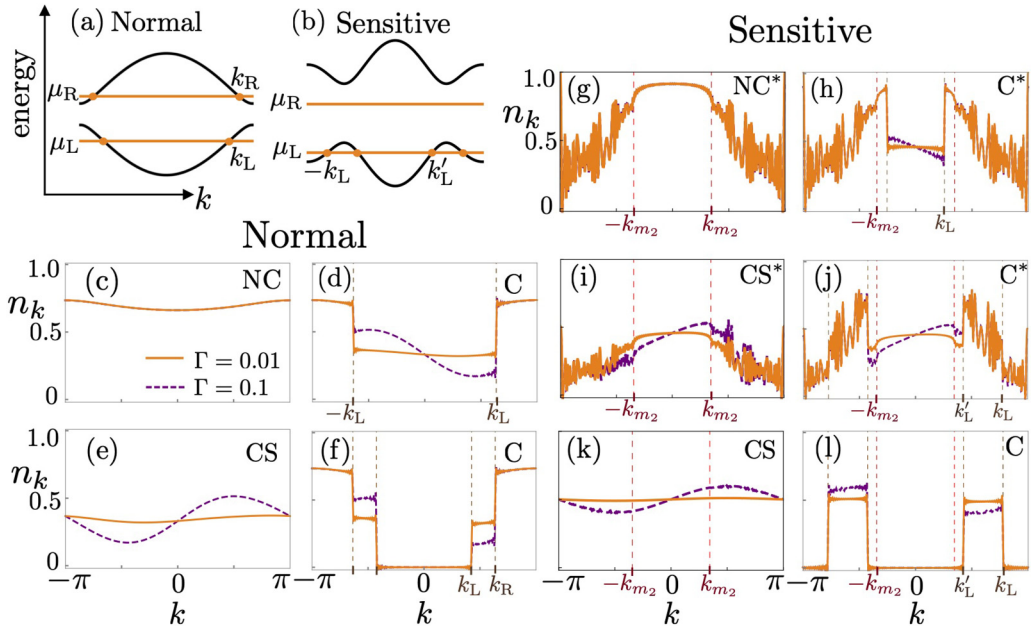

FIG. 5. Distribution of occupations. (a),(b) The momenta $k_{l=\mathrm{L,R}}$ at which the reservoir's chemical potentials $\mu_{l=\mathrm{L,R}}$ cross the dispersion relation. (c)–(f) The excitation number n_k at different phases inside the normal region. (g)–(l) n_k in the sensitive region. k_{m_2} is such that $\varepsilon_{k_{m_2}} = m_2$, with m_2 given in Fig. 3(c).

intimately related to the entropy of a subsystem [41–44]. In analogy, the occupation number of the Bogoliubov excitations, given by Eq. (20), can be used to describe the properties of the asymptotic steady state away from the boundaries. In the open system setting, n_k can be approximated by numerically computing the Fourier transform $\chi_k = \sum_{r\in\Omega} e^{-ik(r-r_0)}\chi_{r,r_0}$, where $\Omega = \{r : L/4 < r < 3L/4\}$ and $r_0 = L/2$, followed by a Bogoliubov transformation. In equilibrium, $\mu_L = \mu_R = 0$, $n_k \simeq 0$ as expected, while in a generic out-of-equilibrium situation, $n_k \neq 0$.

For the Ising model, it was shown that in the CS and NC phases, the n_k is a continuous function of k, while in the C phase, it has discontinuities depending on the reservoir's chemical potentials [22]. These discontinuities happen at the momenta $\pm k_{l=\mathrm{L,R}}$, where the chemical potential $\mu_{l=\mathrm{L,R}}$ crosses the dispersion relation; see Fig. 5(a). These results extent straightforwardly to the XY model in the normal region; see Figs. 5(c)–5(f). Within the O phase, the system behaves as in equilibrium, i.e., $n_k \simeq 0$.

In the sensitive region, there may be two absolute values of momenta, labeled $\pm k_{l=\mathrm{L,R}}$ and $\pm k'_{l=\mathrm{L,R}}$, for which each chemical potential crosses the dispersion relation, as illustrated in Fig. 5(b). Interestingly, we find that n_k has an intrinsic noise in the sensitive region; see Figs. 5(g)–5(j). The noise appears in phases NC*, C*, and CS*, for $|k| > k_{m_2}$, where $\varepsilon_{k_{m_2}} = m_2$ [see Fig. 3(c)]. In Appendix B, we check that the magnitude of the noise in n_k does not diminishes with increasing system sizes. Curiously, the noise vanishes along the line $\mu_L = -\mu_R$, as well as within phases C and CS crossed by this line, as shown in Figs. 5(k) and 5(l), and studied in detail in Appendix B.

Note that n_k is asymmetric upon changing $k \to -k$ for all conducting phases as required to maintain a net energy flow through the chain, as $\varepsilon(k) = \varepsilon(-k)$. Figures 5(c)–5(l) illustrate this feature by showing a larger value of the hybridization, which yields a larger current of energy and consequently to a more asymmetric n_k.

IV. CORRELATION FUNCTIONS

We now consider in more detail the properties of the spin correlation functions, defined in Eq. (21). For $\mathbb{C}^{xx}_{r,r'}$, the generic asymptotic dependence was already given in Eq. (20) and is able to signal the presence of long-range order when $\phi \neq 0$. We give, in Fig. 6(a), a numerical example of this case. On the other hand, when $\phi = 0$, we can extract the correlation length ξ from the exponential decay of $\mathbb{C}^{xx}_{r,r'}$; see Fig. 6(b). Table I shows a summary of the asymptotic dependence of $\mathbb{C}^{xx}_{r,r'}$ in the different phases.

The typical dependence of ϕ and ξ on the chemical potential of the reservoirs is illustrated in Figs. 6(c) and 6(d), showing the remarkable property of a discontinuity in ϕ at the critical point (after extrapolation to the thermodynamic limit) accompanied by a diverging correlation length ξ. Further below we will elaborate on the mixed-order transition in more detail, by also providing an analytical description clarifying its origin.

As shown in Table I, the behavior of $\mathbb{C}^{xx}_{r,r'}$ is not affected by the transition to the sensitive region. However, earlier studies showed how, in the Markovian limit, the CS and NC phases are characterized by a transition, from short- to long-range correlations, when entering the sensitive region. This behavior is reflected by a transition from exponential to power-law decay in $\mathbb{C}^{zz}_{r,r'}$ [13,29]. We observe similar results in the present case, with both nonconducting and saturated phases (CS and NC) showing exponentially decaying correlations in the normal region and power-law decay in the sensitive one (CS* and NC*). Extending the analysis to the highly non-Markovian

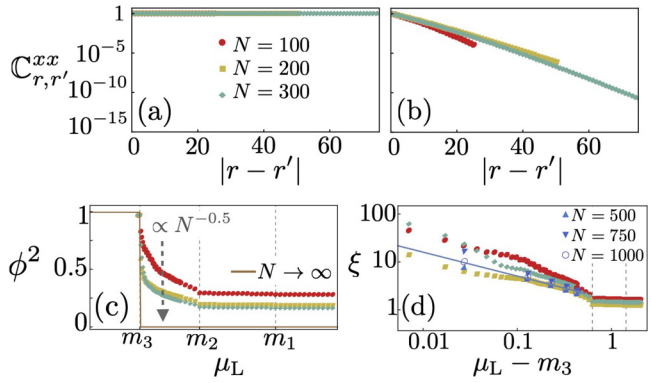

FIG. 6. (a), (b) The correlation $\mathbb{C}^{xx}_{r,r'}$ behavior in the nonequilibrium phases of Fig. 4(b), with fixed $\mu_R = 0$. Long-range order only appears in the ordered phase (O), as exemplified in (a) at the point $|\mu_L| = 0.3 < m_3$, while a typical exponential decay appears in all other phases, as exemplified in (b) for the C* phase at $m_3 < |\mu_L| = 1.3 < m_2$. (c),(d) The mixed-order behavior with a discontinuous order parameter ϕ and diverging correlation length ξ, respectively, in the thermodynamic limit. The straight line in (d) is a guide to the critical exponent $\nu = 1/2$. All panels share the same legends as in (a).

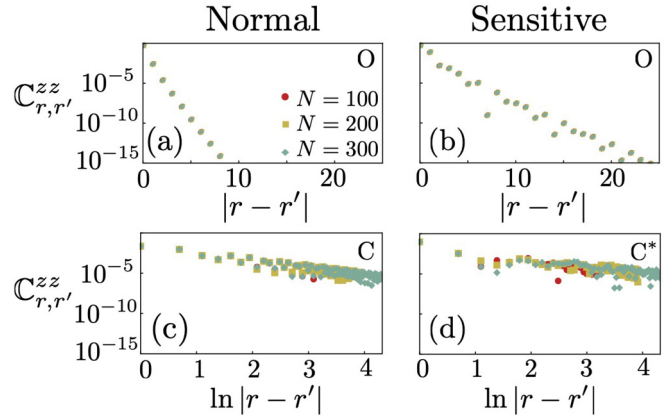

FIG. 7. Correlations $\mathbb{C}^{zz}_{r,r'}$ for the normal (left column) and sensitive (right column) regions; see Fig. 4. We have set (a),(b) $\mu_L = \mu_R = 0$, (c) $m_2 < |\{\mu_L, \mu_R\} = \{2.1, -2.1\}| < m_1$, and (d) $m_3 < |\{\mu_L, \mu_R\} = \{1.3, -1.3\}| < m_2$. These results are summarized in Table I. All panels share the same legends as in (a).

setting, we find that long-range correlations also appear in the conducting phase, with a power-law decay in both normal (C) and sensitive (C*) regions; see Figs. 7(c) and 7(d). These results show that all phases with a noisy excitation number distribution possess power-law decaying zz correlations. The asymptotic behavior of $\mathbb{C}^{zz}_{r,r'}$ in the various phases is summarized in Table I.

A. Mixed-order phase transition

As mentioned earlier, for $\gamma > 1$, the magnetization along the x direction, ϕ, is a good order parameter for the broken-symmetry equilibrium phase. In the open system, ϕ can still be used as the order parameter. However, by changing the chemical potential of the, say, left reservoir, ϕ drops to zero discontinuously as soon as the system reaches the disordered phase. Interestingly, this transition shows a mixed-order behavior where the discontinuity of ϕ is accompanied by a divergence of the correlation length [22]. The divergence occurs as $\xi \propto |\mu_L \pm m_i|^{-\nu}$ when approaching the critical point from the disordered phase ($i = 2, 3$ depending on the values of γ and h). The critical exponent is $\nu = 1/2$, except for special values of the parameters (see Appendix C).

TABLE I. Classification of each phase according to the asymptotic behavior of the correlation functions; the possibilities are exponential (EXP) or power law (PL) decay, and long-range order (LRO).

Phase	$\mathbb{C}^{xx}_{r,r'}(\gamma > 0)$	$\mathbb{C}^{zz}_{r,r'}$
O	LRO	EXP
C/C*	EXP	PL/PL
CS/CS*	EXP	EXP/PL
NC/NC*	EXP	EXP/PL

We have numerically verified that this behavior survives away from $\gamma = 1$, with the same type of dependence of the order parameter and correlation length. In particular, the mixed-order transition with $\nu = 1/2$ is also present in the sensitive region, e.g., at the transitions between O and C* phases in the phase diagram of Fig. 4(b). We show in Figs. 6(c) and 6(d) an example of the numerical analysis of the order parameter and correlation length in the sensitive region. The main difference compared to the normal region is that here finite-size effects are much stronger, which is consistent with the sensitive dependence on N of the rapidity spectrum and occupation numbers; see Figs. 3 and 5.

To derive the value of the critical exponent ν, we consider the explicit form of the correlation function in terms of a Toeplitz determinant [31,38],

$$\langle \sigma^x_r \sigma^x_{r+n} \rangle = \begin{vmatrix} D_0 & D_{-1} & . & . & D_{-n+1} \\ D_1 & D_0 & . & . & . \\ . & . & . & . & . \\ . & . & . & D_0 & D_{-1} \\ D_{n-1} & . & . & D_1 & D_0 \end{vmatrix}, \tag{24}$$

where D_n is given by

$$D_n = \int \frac{dk}{2\pi} e^{-ink} \sqrt{\frac{1 - (h/J)e^{ik}}{1 - (h/J)e^{-ik}}} (1 - n_k - n_{-k}). \tag{25}$$

The asymptotic dependence can be obtained from Szego's lemma, leading to the following expression for the correlation length:

$$\xi^{-1} = -\frac{1}{2\pi} \int_0^{2\pi} \ln [1 - n_k - n_{-k}] dk. \tag{26}$$

Here, the difference from the standard treatment of the transverse-field Ising chain [31,38] is simply that the occupation numbers n_k are kept generic, and thus are allowed to assume any nonequilibrium distribution induced by the external reservoirs. For example, Eq. (26) takes into account that in general $n_k \neq n_{-k}$, as shown by Fig. 5 with a large hybridization energy. By substituting the Fermi distribution,

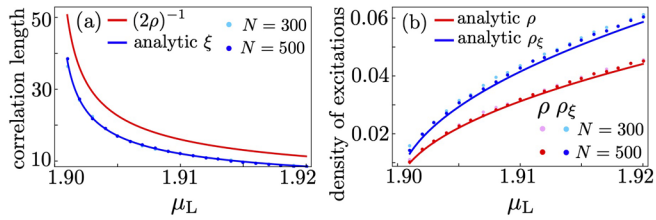

FIG. 8. (a) The correlation length of the Ising model ($\gamma = 1$), computed at weak transverse field ($h/J = -0.05$) and approaching the critical point $m_1 = 1.9$ from the disordered phase, with $\mu_R = 0$. The numerical results (dots) agree well with the blue (lower) curve, given by Eq. (28). The red (upper) curve is from the equilibrium relation $\xi^{-1} = 2\rho$, where $\rho = \int_0^{2\pi} \frac{dk}{2\pi} n_k$ is the density of excitations. (b) Comparison between the numerically computed ρ (upper dots) and the modified density ρ_ξ (lower dots), defined in Eq. (30). The solid curves were obtained by assuming a parabolic dispersion and $n_k \simeq n_\pi$ within the occupied region.

Eqs. (25) and (26) recover the known equilibrium expressions at finite temperature [38,45].

Applying Eq. (26) to the critical point, we first assume, as in Fig. 5(a), that the minimum of the quasiparticle dispersion occurs at $k = \pi$. Furthermore, if μ_R is inside the gap, the critical point is at $\mu_L = m_2$. Close to the critical point, the only occupied states are in a small range, $k \in [\pi - \Delta k_L, \pi + \Delta k_L]$, around the minimum of ε_k, and thus we can approximate the quasiparticle dispersion as parabolic, giving $\Delta k_L \propto \sqrt{\mu_L - m_2}$. This dependence of Δk_L is directly related to the critical exponent $\nu = 1/2$. More precisely, Δk_L close to the critical point is given by

$$\Delta k_L \simeq \sqrt{\frac{|1 + h/J|}{\gamma^2 - h/J - 1}(\mu_L - m_2)}, \tag{27}$$

and we can set $n_k \simeq n_{k=\pi}$ in the small integration interval of Eq. (26), leading to

$$\xi^{-1} \simeq -\frac{\Delta k_L}{\pi} \ln[1 - 2n_\pi]. \tag{28}$$

This expression clearly shows how the divergence of ξ is due to the shrinking of the region of nonzero occupation. We show in Fig. 8 that this theory is accurate by a direct comparison to the numerical results.

After having clarified the origin of the critical exponent $\nu = 1/2$, it is interesting to compare the behavior of the open chain to the temperature dependence of the equilibrium system. In the latter case, an ordered phase is only allowed at zero temperature and the order disappears at any arbitrarily small temperature $T > 0$. The sudden disappearance of the ordered state is related to the presence of thermal excitations and is analogous to the vanishing of ϕ induced by the nonequilibrium chemical potentials, as soon as either μ_L or μ_R overcomes the gap. Furthermore, similarly to the nonequilibrium system, the correlation length diverges when $T \to 0$. As it turns out, in the low-temperature limit, ξ can be related in a simple way to the density of excitations $\rho = \int_0^{2\pi} \frac{dk}{2\pi} n_k$:

$$\xi^{-1} = 2\rho \quad \text{(low temperature)}. \tag{29}$$

This expression follows immediately from Eq. (26) since $n_k = n_{-k} \ll 1$ when $T \to 0$, and can also be understood by a simple argument in terms of a dilute gas of domain-wall excitations [45].

A naive application of Eq. (29) to the nonequilibrium system is shown in Fig. 8. Although Eq. (29) predicts the correct critical exponent $\nu = 1/2$, there is a clear disagreement with the numerical results. This failure of Eq. (29) can be explained from the nonvanishing value of n_k around the minimum of ε_k (say, $k = \pi$): in both the low-temperature limit and the nonequilibrium system, we have $\rho \to 0$ at the critical point, which results in a diverging correlation length. However, in the first case, we have $n_k \to 0$, while for the nonequilibrium system, n_π remains finite and the vanishing of ρ is due to the shrinking of Δk_L. Instead of the density ρ, we can consider a "modified" density,

$$\rho_\xi = -\frac{1}{4\pi} \int_0^{2\pi} \ln[1 - n_k - n_{-k}] dk, \tag{30}$$

which follows naturally from Eq. (26) by requiring that a relation similar to the equilibrium system at low temperature is satisfied, $\xi^{-1} = 2\rho_\xi$. It is easy to see that close to the critical point, we have $\rho_\xi \simeq -(\ln[1 - 2n_\pi]/2n_\pi)\rho$, which differs from ρ by a nontrivial multiplicative factor. An interesting exception, discussed more extensively in Appendix C, occurs for $J = h/2$, when $n_\pi = 0$ and the relation between ξ and ρ is Eq. (29), as in equilibrium. At $J = h/2$, the vanishing of n_k also affects the value of the critical exponent, which is $\nu = 5/2$ instead of $1/2$.

The above arguments can be adapted to other parameter regimes. In particular, the discussion is almost unchanged for $h/J < \min[0, \gamma^2 - 1]$, when the dispersion minimum is at $k = 0$. Instead, the treatment of the sensitive phase with $|\gamma| < 1$ is more delicate. First, as shown in Fig. 5(b), the dispersion is characterized by two minima instead of one. More importantly, n_k appears to be highly pathological when $N \to \infty$, when the occupation numbers undergo wild oscillations. Despite these differences, numerical evaluation of the critical exponent still gives $\nu = 1/2$, and thus we conjecture that a suitable average of n_k is well defined,

$$\overline{n_k} = \lim_{\Delta k \to 0} \lim_{N \to \infty} \frac{1}{\Delta k} \int_{k - \frac{\Delta k}{2}}^{k + \frac{\Delta k}{2}} n_{k'} dk'. \tag{31}$$

Then, the critical exponent would be determined through Eq. (28) in a way analogous to the regular case, i.e., the critical exponent would correspond to the shrinking of the occupied regions around the minima, explaining the persistence of $\nu = 1/2$ in this phase.

B. z correlations

As summarized in Table I, $\mathbb{C}^{zz}_{r,r'}$ displays a power-law decay in several of the allowed phases. We focus here on the the nonsensitive region, where this behavior can be understood from the well-known power-law decay of density-density correlations of noninteracting fermions. In fact, through the fermionic mapping, $\mathbb{C}^{zz}_{r,r'}$ is equivalent to a density-density correlation function,

$$\mathbb{C}^{zz}_{r,r'} = 4(\langle \hat{c}^\dagger_r \hat{c}_r \hat{c}^\dagger_{r'} \hat{c}_{r'} \rangle - \langle \hat{c}^\dagger_r \hat{c}_r \rangle \langle \hat{c}^\dagger_{r'} \hat{c}_{r'} \rangle). \tag{32}$$

In the C phase, at least one of the reservoirs has its chemical potential within the range of the quasiparticle energy spectrum. Then, the correlation function is expected to have a power-lay decay with oscillating character, similar to a simple one-dimensional (1D) Fermi gas where it decays as $|r-r'|^{-2}$ and oscillates with wave vector $2k_F$, with k_F the Fermi wave vector (see, e.g., Ref. [46]).

In our case, we express the correlation function through the Bogoliubov excitations $\hat{\gamma}_k$ of the translational-invariant system (which is appropriate in the thermodynamic limit). The corresponding occupation numbers are defined in Eq. (20) and give

$$\mathbb{C}^{zz}_{r,0} = \left|\int_{-\pi}^{\pi}\frac{dk}{2\pi}e^{ikr}(n_{-k}+n_k-1)\sin 2\theta_k\right|^2 - \left|\int_{-\pi}^{\pi}\frac{dk}{2\pi}e^{ikr}[(n_k+n_{-k}-1)\cos 2\theta_k+(n_k-n_{-k})]\right|^2. \tag{33}$$

If, for simplicity, we assume $n_k \simeq n_{-k}$ (which is justified in the limit of vanishing hybridization energy Γ), the occupation numbers have discontinuities at $k=\pm k_i$, induced by the left and right reservoirs ($i=L,R$). When $k_i r \gg 1$, we can extract the leading contribution to Eq. (33) induced by the discontinuous jumps Δn_{k_i} of n_k, defined by $\partial_k n_k = \sum_{i=\mathrm{L,R}}\Delta n_{k_i}[\delta(k+k_i)-\delta(k-k_i)]$:

$$\mathbb{C}^{zz}_{r,0} \simeq \frac{4}{\pi^2 r^2}\left[\left(\sum_{i=\mathrm{L,R}}\Delta n_{k_i}\sin 2\theta_{k_i}\cos k_i r\right)^2 - \left(\sum_{i=\mathrm{L,R}}\Delta n_{k_i}\cos 2\theta_{k_i}\sin k_i r\right)^2\right], \tag{34}$$

which simplifies to

$$\mathbb{C}^{zz}_{r,0} \simeq \frac{4\Delta n_{k_R}^2}{\pi^2 r^2}\left(\cos^2 k_R r - \cos^2 2\theta_{k_R}\right), \tag{35}$$

when there is a single Fermi surface (here, induced by $i=R$). The above expressions display the expected $1/r^2$ decay and oscillatory dependence. As shown in Fig. 9, we find a good agreement between Eq. (35) and the numerical results.

To better characterize the oscillatory dependence, we have also studied the Fourier transform,

$$\mathbb{C}^{zz}_{k} \equiv \frac{1}{\sqrt{N}}\sum_{r-r'}e^{-ik(r-r')}\mathbb{C}^{zz}_{r,r'}, \tag{36}$$

which is shown in Fig. 10 for two representative cases. With a single Fermi surface (left panels), we find dominant nonanalytic features at $k=0, 2k_R$, in agreement with Eq. (35). We also find smaller discontinuities in $\partial_k\mathbb{C}^{zz}_k$ at higher harmonics, $k=4k_R, 6k_R$, which are not captured by the leading-order approximation given by Eq. (35). With two Fermi surfaces (right panels), we find the expected singularities at $k=0, 2k_{L,R}$. However, there are additional features at $\partial_k\mathbb{C}^{zz}_k$ at $k=k_L\pm k_R$, which are in agreement with Eq. (34). As seen there, the correlation function is not simply a sum of $i=L,R$ contributions, but involves interference terms between the two Fermi surfaces.

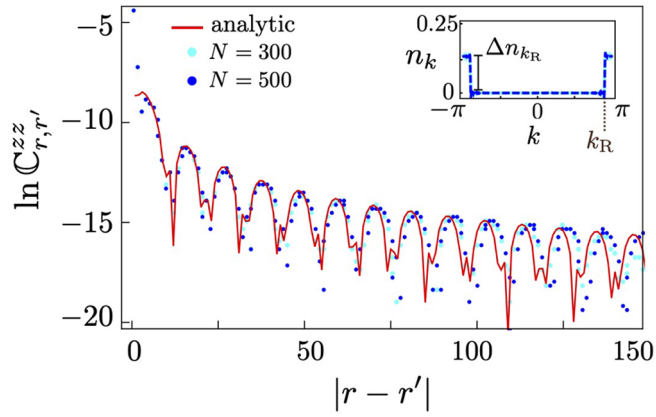

FIG. 9. Comparison between numerical results for $\mathbb{C}^{zz}_{r,r'}$ (dots) and the analytic approximation given by Eq. (35) (red curve). The values $\Delta n_{k_R}\simeq 0.1$ and $k_R\simeq 2.85$ were extracted numerically from n_k, as shown in the inset. We used $h=0.2$, $\gamma=1$, $\mu_L=0.5<m_2$, and $\mu_R=1.62\gtrsim m_3$.

Finally, we comment on the power-law dependence of $\mathbb{C}^{zz}_{r,r'}$ in the sensitive region. Away from the ordered phase, we find a power-law decay $|r-r'|^{-s}$ where, however, the exponent is generally different from $s=2$ (we often find $s<2$) and depends on system parameters. This behavior is most likely related to the singular nature of n_k, which from our numerical evidence is characterized by a complex pattern of closely spaced discontinuities (see, e.g., Fig. 5). Such discontinuities will contribute to the square brackets of Eq. (34) in a way that is difficult to compute explicitly (the summation index i should become a continuous parameter) and might be able to modify the exponent s. This interpretation is confirmed by the survival of the power-lay decay in the NC* and CS* regions, where the chemical potentials $\mu_{L,R}$ do not cross the quasiparticle bands, and thus an exponential decay might be expected. Instead, Figs. 5(g) and 5(i) show that a discontinuous dependence of n_k can be found in these regions as well, in agreement with the observed power-law dependence of $\mathbb{C}^{zz}_{r,r'}$. Finally, the simple discontinuities of Fig. 5(l) result in the regular value $s=2$.

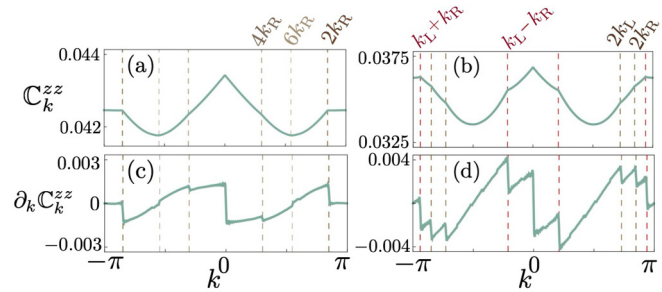

FIG. 10. Within the phase diagram of Fig. 4(a), here (a) and (b) show the Fourier transform of $\mathbb{C}^{zz}_{r,r'}$ [see Eq. (36)] for points inside the C phase, namely, (a) at $\{\mu_L,\mu_R\}=\{-2.9,-2.1\}$ and (b) at $\{\mu_L,\mu_R\}=\{-1.9,-2.1\}$. (c),(d) Their respective derivatives. In the left column, we considered the case with only nonzero k_R, while the right column considers nonzero k_L and k_R. We have computed these results for a system size of $N=500$ sites.

V. ENTROPY AND MUTUAL INFORMATION

In this section, we study the entropy of the steady state within the different phases identified above. For a segment of ℓ sites in the middle of the chain, the entropy is given by

$$E_\ell = -\mathrm{Tr}[\hat{\rho}_\ell \ln(\hat{\rho}_\ell)] = -\mathrm{tr}[\chi_\ell \ln \chi_\ell], \tag{37}$$

where $\hat{\rho}_\ell$ is the reduced density matrix and χ_ℓ is the single-particle correlation matrix restricted to the subsystem of ℓ sites. While, for the fermionic system the second equality follows from the noninteracting nature of the problem, this expression was also shown to hold for the spin chain [47]. In the thermodynamic limit ($N \to \infty$), the entropy of the segment of a translational-invariant system is expected to obey the general scaling law [48]

$$E_\ell = l_0 \ell + c_0 \ln(\ell) + c_1, \tag{38}$$

where l_0, c_0, and c_1 are ℓ-independent real constants. For the ground state of gapped systems, $l_0 = c_0 = 0$, following the so-called area law, while gapless fermions and spin chains show a universal logarithmic behavior with $c_0 = 1/3$. This result is a consequence of the violation of the area law in $1+1$ conformal theories, in which case $c_0 = c/3$, where c is the central charge [47,49]. For a nonequilibrium Fermi gas, it was shown that both l_0 and c_0 can be nonzero [50,51], and that c_0 depends on the system-reservoir coupling and is a nonanalytic function of the bias [51]. The coefficient c_0 is most easily extracted from the mutual information, $\mathcal{I}(A,B) \equiv E(\hat{\rho}_A) + E(\hat{\rho}_B) - E(\hat{\rho}_{A+B})$, of two adjacent segments A and B of size $\ell/2$, since

$$\mathcal{I}_\ell \simeq c_0 \ln(\ell) + c_2. \tag{39}$$

For the transverse-field Ising model, in Fig. 4(a), all phases, except O, have been shown to have extensive entropy (i.e., $l_0 \neq 0$) [22]. This is due to the presence of a finite fraction of excitations, which are absent in the ordered phase. In addition, it was found that $c_0 \neq 0$ in the C phase due to the presence of discontinuities in n_k.

In Fig. 11, we show the generalization of the previous results to the XY chain and including the sensitive region of the phase diagram. Figure 11(a) shows l_0 for both normal and sensitive regions. In both cases, l_0 follows the expected value [51]:

$$l_0 = \int \frac{dk}{2\pi} - [n_k \ln n_k + (1-n_k)\ln(1-n_k)]. \tag{40}$$

On the other hand, $\mathcal{I}_\ell$ does differ qualitatively in the normal and sensitive regions. As mentioned earlier, logarithmic corrections come from discontinuities in n_k. If n_k has no discontinuities such as in the O and saturated normal phases, c_0 vanishes. Figure 11(b) depicts c_0 in the normal region. The right inset shows that the leading term of $\mathcal{I}_\ell$ in Eq. (39) is indeed logarithmic in the large-ℓ limit. In principle, for conducting nonsaturated phases in the normal region, c_0 can be computed using the Fisher-Hartwing conjecture [48].

The presence of noise in n_k within the sensitive region changes the previous picture. The left inset of Fig. 11(b) shows that $\mathcal{I}_\ell$ is no longer of the form given in Eq. (39). It is tempting to interpret this result as a collection of discontinuities of n_k whose number increases with system size. However, due to the noisy form of n_k, it is difficult to give a precise meaning to this picture. Moreover, with the system sizes that we could attain, it was not possible to determine the functional form of this correction with ℓ. Note that a supralogarithmic contribution in $\mathcal{I}_\ell$ is always present in the sensitive region even for the CS* and NC* phases.

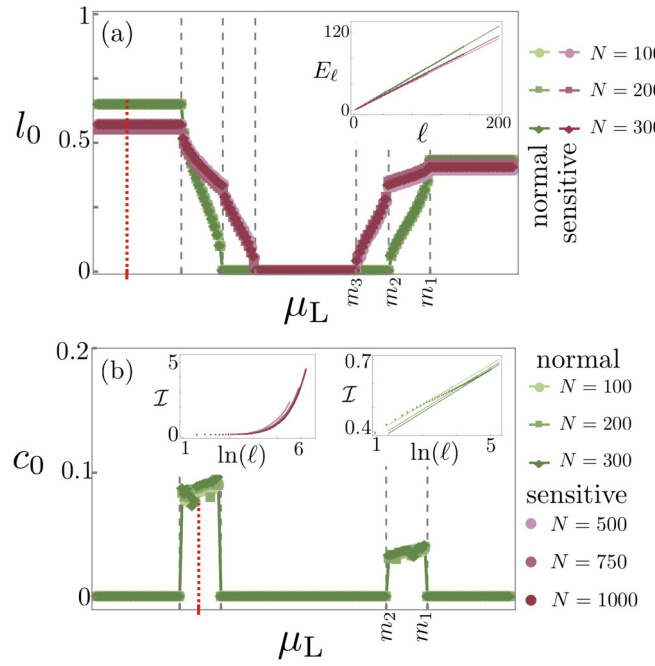

FIG. 11. (a) Linear coefficient l_0, obtained from the entropy scaling law, for a range of μ_L across the lines depicted in the phase diagrams of Fig. 4. The inset illustrates the typical fitting $E_\ell \times \ell$, where the value of μ_L used is denoted by the dotted red line. (b) Similar results for the logarithmic coefficient c_0, obtained from Eq. (39), for the same range of μ_L. The inset on the right illustrates the typical fitting $\mathcal{I} \times \ln(\ell)$, where the value of μ_L is denoted by the dotted red line. In the sensitive region (left inset), the mutual information is superlogarithmic.

VI. DISCUSSIONS

We have studied the steady state of a transverse-field XY-spin chain at zero temperature in a nonequilibrium setting by coupling the ends of the chain to reservoirs which can be held at different magnetic potentials. Our approach is based on a Jordan-Wigner mapping and a Keldysh Green's function treatment of the resulting nonequilibrium interaction-free fermionic system.

This allows us to study the steady states of the model as a function of the magnetic potentials including the equilibrium and Markovian limits. For magnetic potentials whose magnitudes remain smaller than the spectral gap, the equilibrium-ordered state persists and the correlation function of the order parameter displays long-range order. Away from this phase, the order parameter correlations decay exponentially. As μ_L or μ_R reaches the spectral gap, the transition from equilibrium to a current-carrying state occurs through

a mixed-ordered transition, where the order parameter vanishes discontinuously while the correlation length diverges. This out-of-equilibrium phenomena was previously observed in Ref. [22]. Our present results establish that this behavior is generic to all order/disorder phase transitions of the XY chain.

For large $|\mu_L|$ and $|\mu_R|$, we recover the Markovian limit. We identify the two qualitatively different behaviors previously reported using a Lindblad master-equation approach [13,39]. We refer to these as the (i) sensitive region, featuring algebraic decaying correlations in the transverse (i.e., z) direction, and (ii) normal region, where these correlations decay exponentially.

Besides the equilibrium and Markovian phases, we identify additional current-carrying phases. Their properties can be easily understood by studying the quasiparticle excitation number n_k. By analyzing this quantity, we were able to compute the critical exponent of the diverging correlation length at the transition, confirming analytically the results of Ref. [22]. The behavior of the transverse correlation function in the normal region is explained in terms of a physical effect, which is similar to Friedel oscillations in metals, here observed in a nonequilibrium setting.

For steady-state phases within the sensitive region, n_k is noisy, for k belonging to the intervals of momentum where the dispersion relation allows four propagating modes. This noise cannot be interpreted as a finite-size feature since n_k, within these regions, does not converge to a thermodynamic limit. Since the transverse correlation function is related to the Fourier transform of n_k, the pathologies of this function explain the nonexponential decay of transverse correlations in the sensitive region.

We have also analyzed the behavior of the entropy of a segment of the steady state with its length. As expected for a mixed state, the steady-state entropy is extensive and follows its predicted semiclassical value. In the normal region, whenever the chemical potential lies within one of the bands, there is a logarithmic component that is reminiscent of the area-law violation occurring in equilibrium gapless states. As reported for other nonequilibrium setups [51], the logarithmic coefficient depends on the discontinuities of n_k. In the sensitive region, corrections to the extensive contribution turn out to be superlogarithmic.

The analysis presented here generalizes our earlier findings on the transverse-field Ising case to the anisotropic XY chain and, thus, extends the class of spin chains which display far-from-equilibrium critical behavior, reflected in a divergent correlation length, that is absent in equilibrium. Thus, the present work suggests that these findings may reflect common features of a wide class of quantum statistical models. A common feature of the models discussed in the present context is their equivalence to interaction-free fermions under a Jordan-Wigner transformation. This naturally poses the question if there exists a finite region in model space around these XY chains where similar nonequilibrium behavior ensues, or whether their nonthermal behavior is singular. The Jordan-Wigner transformation is limited to 1D systems. Yet, it would be desirable to understand how the nonequilibrium phases that we have identified generalize in higher dimensions.

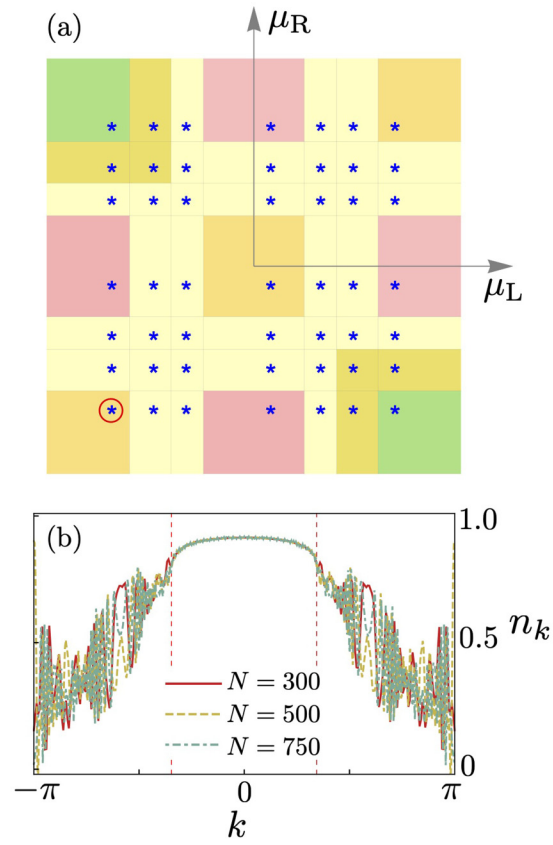

FIG. 12. (a) Repeat of the phase diagram of Fig. 4(b). The blue stars mark the parameters used in Fig. 13. (b) The persistent noise in the occupation number, computed for different system sizes, with the set of parameters indicated by the circled blue star on the phase diagram.

In equilibrium, interaction-free or quadratic models are commonly associated with fixed point behavior within a field-theoretic description of criticality. This enables one to categorize a wide class of systems into universality classes, with respect to the fixed points. Away from equilibrium, such a categorization is not available. Our results thus offer a vantage point for the construction of a wider class of models that share the same out-of-equilibrium behavior. A better understanding of the universality of far-from-equilibrium critical behavior should prove beneficial for the construction of a field-theoretic description of quantum critical matter far from equilibrium.

ACKNOWLEDGMENTS

We gratefully acknowledge helpful discussions with T. Prosen, V. R. Vieira, and R. Fazio. P. Ribeiro acknowledges support by FCT (Grant No. UID/CTM/04540/2019). S. Kirchner acknowledges support by the NSFC (Grant No. 11774307) and the National Key R&D Program of the MOST of China (Grant No. 2016YFA0300202). S.C. acknowledges support from the National Key R&D Program of MOST China (Grant No. 2016YFA0301200), the National Science Association Funds (Grant No. U1930402), and NSFC (Grants No. 11974040 and No. 1171101295).

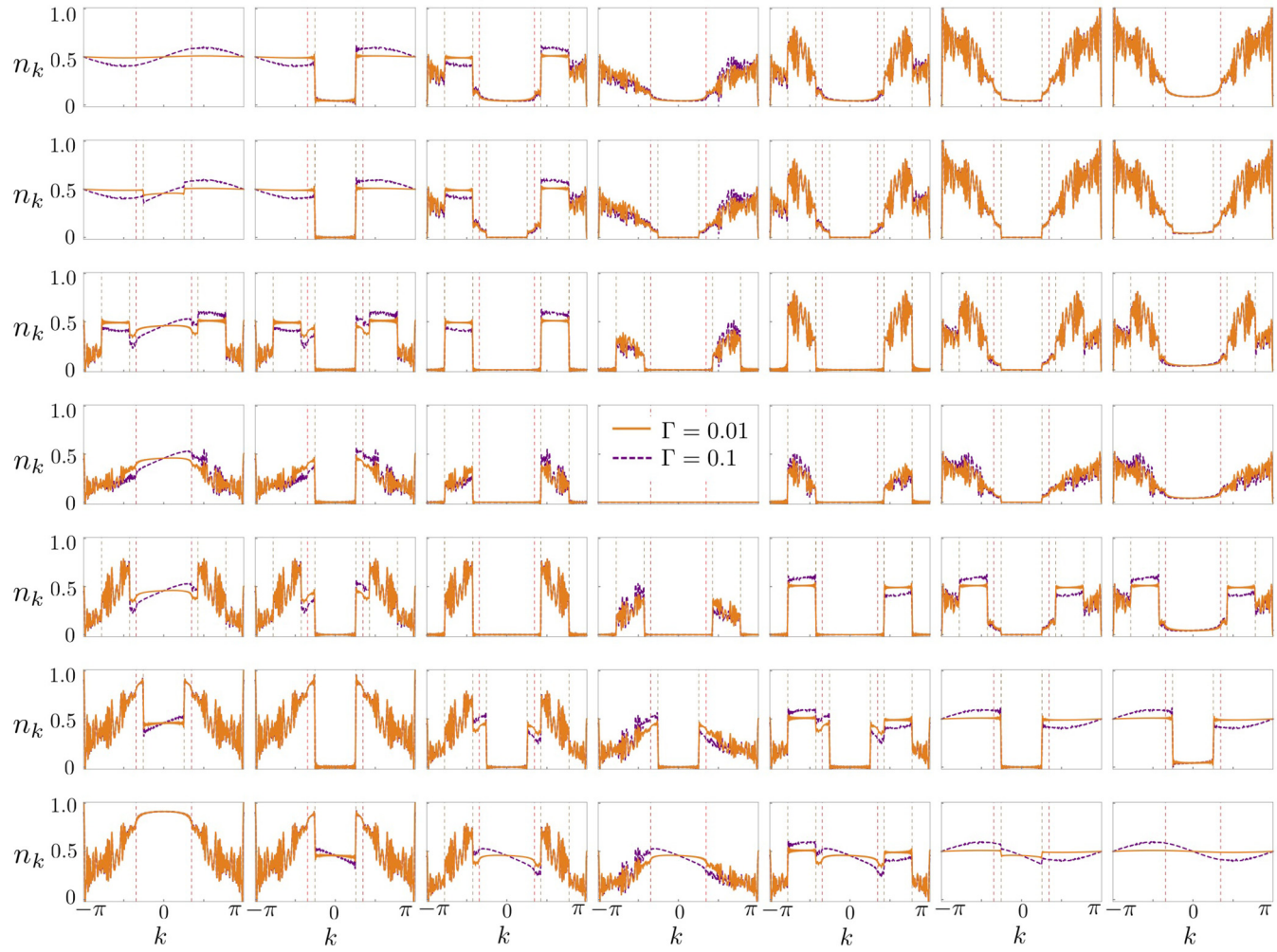

FIG. 13. Excitation number n_k in the sensitive region for different phases. Each plot represents a different set of parameters $\{\mu_L, \mu_R\}$ marked on the phase diagram in Fig. 12(a) disposed in the same order. We have computed it for a system size of $N = 500$ sites. The vertical dashed lines represent either the momentum k_{m_2} or k_L; see Figs. 3(c), 5(a), and 5(b).

APPENDIX A: METHOD DETAILED

The single-particle density matrix in Eq. (16) is explicitly given by

$$\boldsymbol{\chi} = \frac{1}{2} + \sum_{l=\mathrm{L,R}} \sum_{\alpha\beta} |\alpha\rangle\langle\beta|\langle\tilde{\alpha}|[\boldsymbol{\gamma}_l I_l(\lambda_\alpha, \lambda_\beta^*) - \hat{\boldsymbol{\gamma}}_l I_l(-\lambda_\alpha, -\lambda_\beta^*)]|\tilde{\beta}\rangle, \tag{A1}$$

where $I_l(z, z') = -\frac{1}{\pi}\frac{g(z-2m_l)-g(z'-2m_l)}{z-z'}$, with $g(z) = \ln\{-i\mathrm{sgn}[\mathrm{Im}(z)]z\}$, and the matrices $\boldsymbol{\gamma}_l$ are defined in Eq. (13). Here we assumed that $\boldsymbol{K}$ in Eq. (13) is diagonalizable, having right and left eigenvectors $|\alpha\rangle$ and $\langle\tilde{\alpha}|$ with associated eigenvalues λ_α.

The energy drained to the left reservoir is $\mathcal{J}_e = -i\langle[H, H_L]\rangle$, which equals the steady-state energy current in any cross section along the chain and thus can be obtained as a function of $\boldsymbol{\chi}$. Explicitly, the energy flow can be obtained as $\mathcal{J}_e = -\frac{1}{2}\mathrm{Tr}[\boldsymbol{J}_r\boldsymbol{\chi}] \forall\, r$, given by Eq. (23), with

$$\boldsymbol{J}_r = -2ihJ[(1+\boldsymbol{S})|r-1\rangle\langle r|(1+\boldsymbol{S}) - \mathrm{H.c.}]\,. \tag{A2}$$

The linear and nonlinear thermal conductivities, as well as other thermoelectric properties of the chain, are determined by $\mathcal{J}_e$.

Two-point correlation

Let us further analyze the two-point correlation function in Eq. (21), which can also be found in terms of $\boldsymbol{\chi}$. To this end, we have extended the equilibrium expressions [31] to general nonequilibrium conditions,

$$\mathbb{C}^{xx}_{r,r'} = \det[i(2\boldsymbol{\chi}_{[r,r']} - 1)]^{\frac{1}{2}}, \tag{A3}$$

for $r > r' + 1$, where $\boldsymbol{\chi}_{[r,r']}$ is a $2(r-r')$ matrix obtained as the restriction of $\boldsymbol{\chi}$ to the subspace in which $\mathbb{P}^T_{rr'} = \sum_{u=r'+1}^{r-1}(|u\rangle\langle u| + |\hat{u}\rangle\langle\hat{u}|) + |r_+\rangle\langle r_+| + |r'_-\rangle\langle r'_-|$, with $|r_\pm\rangle = (|r\rangle \pm |\hat{r}\rangle)/\sqrt{2}$, acts as the identity, and $|r\rangle$ and $|\hat{r}\rangle \equiv \boldsymbol{S}|r\rangle$ are single-particle and hole states.

APPENDIX B: EXCITATION NUMBER

The intriguing results of the occupation number, computed in Sec. III D, deserve a more detailed analysis, as follows. As

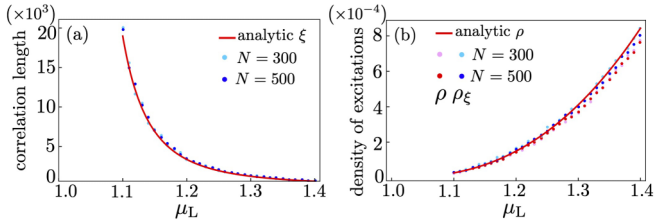

FIG. 14. (a) Correlation length of the Ising model ($\gamma = 1$) for the special case $h/J = 0.5$ and approaching the critical point $m_2 = 1$ from the disordered phase (C), with $\mu_R = 0$. The dots and continuous line compare the numerical result, given by Eq. (22), to the analytic result, given by Eq. (C2), respectively. (b) Density of excitations ρ and ρ_ξ, given by Eq. (30). The continuous line shows the analytic result for ρ, computed from Eq. (C2) as $\rho = \xi^{-1}/2$. In the analytic formulas, we have used the educated guess $c = \pi/5$!.

discussed in the manuscript, the occupation number shows a noise behavior in some of the phases. The marks in Fig. 12(a) indicate the representative sets $(\mu_L \mu_R)$ for which the occupation numbers are given in Fig. 13, providing the reader with a complete view of all possible cases. Here we have set the system in the sensitive region with transverse magnetic field $h/J = 0.2$ and anisotropy $\gamma = 0.5$. The marks are at the points μ_L, $\mu_R = \{\pm 2.7, \pm 1.9, \pm 1.3, +0.3 \text{ or } -0.3\}$.

As discussed in the manuscript, here we clearly see that the noise is present on the phases around the axis $\mu_L = \mu_R$, while it vanishes around the axis $\mu_L = -\mu_R$. The noise only appears for $|k| > k_{m_2}$; see Fig. 3(c). In addition, it is persistent even in the thermodynamic limit, as shown in Fig. 12(b).

APPENDIX C: CORRELATION LENGTH at $h/J = 0.5$

When $h/J = 0.5$, it was observed that $n_{k=\pi} = 0$ [22], and thus the derivation of Eq. (28) should be modified. Interestingly, around $k = \pi$, we find that n_k has a leading term of the form

$$n_k \simeq c(k - \pi)^4, \tag{C1}$$

where the vanishing of the quadratic term and the value of c could only be obtained numerically. In the limit of a small Δk_L, Eq. (26) yields

$$\xi^{-1} \simeq \frac{c}{\pi} \int_{-\Delta k_L}^{\Delta k_L} x^4 dx = \frac{2c}{5\pi} \Delta k_L^5. \tag{C2}$$

Finally, from the expression of Δk_L in Eq. (27), we immediately see that the critical exponent is $\nu = 5/2$. It is also worth mentioning that since n_k becomes vanishingly small approaching the critical point, Eq. (30) coincides with the regular density and the relation $\xi^{-1} = 2\rho$ is still valid. Figure 14 shows the comparison of these results with the numerical calculations.

[1] H. Pothier, S. Guéron, N. O. Birge, D. Esteve, and M. H. Devoret, Phys. Rev. Lett. **79**, 3490 (1997).
[2] A. Anthore, F. Pierre, H. Pothier, and D. Esteve, Phys. Rev. Lett. **90**, 076806 (2003).
[3] Y.-F. Chen, T. Dirks, G. Al-Zoubi, N. O. Birge, and N. Mason, Phys. Rev. Lett. **102**, 036804 (2009).
[4] J.-P. Brantut, C. Grenier, J. Meineke, D. Stadler, S. Krinner, C. Kollath, T. Esslinger, and A. Georges, Science **342**, 713 (2013).
[5] M. Büttiker and R. Landauer, Phys. Rev. Lett. **49**, 1739 (1982).
[6] G. Stefanucci and R. van Leeuwen, *Nonequilibrium Many-Body Theory of Quantum Systems: A Modern Introduction* (Cambridge University Press, Cambridge, 2013).
[7] S. Datta, H. Ahmad, and M. Pepper, *Electronic Transport in Mesoscopic Systems*, Cambridge Studies in Semiconductor Physics (Cambridge University Press, Cambridge, 1997).
[8] Y. Imry, *Introduction to Mesoscopic Physics*, Mesoscopic Physics and Nanotechnology (Oxford University Press, Oxford, 2002).
[9] H. Aoki, N. Tsuji, M. Eckstein, M. Kollar, T. Oka, and P. Werner, Rev. Mod. Phys. **86**, 779 (2014).
[10] D. B. Gutman, Y. Gefen, and A. D. Mirlin, Phys. Rev. Lett. **101**, 126802 (2008).
[11] D. B. Gutman, Y. Gefen, and A. D. Mirlin, Phys. Rev. B **80**, 045106 (2009).
[12] S. Ngo Dinh, D. A. Bagrets, and A. D. Mirlin, Phys. Rev. B **81**, 081306(R) (2010).
[13] T. Prosen and I. Pižorn, Phys. Rev. Lett. **101**, 105701 (2008).
[14] T. Prosen and B. Žunkovič, New J. Phys. **12**, 025016 (2010).
[15] T. Prosen, Phys. Rev. Lett. **107**, 137201 (2011).
[16] T. Prosen, Phys. Rev. Lett. **112**, 030603 (2014).
[17] P. Ribeiro and V. R. Vieira, Phys. Rev. B **92**, 100302(R) (2015).
[18] P. Ribeiro and V. R. Vieira, in *Symmetry, Spin Dynamics and the Properties of Nanostructures* (World Scientific, Singapore, 2015), pp. 86–111.
[19] B. Bertini, M. Collura, J. De Nardis, and M. Fagotti, Phys. Rev. Lett. **117**, 207201 (2016).
[20] O. A. Castro-Alvaredo, B. Doyon, and T. Yoshimura, Phys. Rev. X **6**, 041065 (2016).
[21] E. Arrigoni, M. Knap, and W. von der Linden, Phys. Rev. Lett. **110**, 086403 (2013).
[22] T. O. Puel, S. Chesi, S. Kirchner, and P. Ribeiro, Phys. Rev. Lett. **122**, 235701 (2019).
[23] D. J. Thouless, Phys. Rev. **187**, 732 (1969).
[24] A. Bar and D. Mukamel, Phys. Rev. Lett. **112**, 015701 (2014).
[25] A. Fronczak, P. Fronczak, and A. Krawiecki, Phys. Rev. E **93**, 012124 (2016).
[26] J.-C. Anglès d'Auriac and F. Iglói, Phys. Rev. E **94**, 062126 (2016).
[27] R. Juhász and F. Iglói, Phys. Rev. E **95**, 022109 (2017).
[28] R. Alert, P. Tierno, and J. Casademunt, Proc. Natl. Acad. Sci. **114**, 12906 (2017).
[29] B. Žunkovič and T. Prosen, J. Stat. Mech.: Theory Expt. (2010) P08016.
[30] S. Ajisaka, F. Barra, and B. Žunkovič, New J. Phys. **16**, 033028 (2014).
[31] E. Lieb, T. Schultz, and D. Mattis, Ann. Phys. **16**, 407 (1961).
[32] A. Y. Kitaev, Phys. Usp. **44**, 131 (2001).
[33] F. Meier and D. Loss, Phys. Rev. Lett. **90**, 167204 (2003).

[34] K. Nakata, P. Simon, and D. Loss, J. Phys. D **50**, 114004 (2017).
[35] S. Hoffman, D. Loss, and Y. Tserkovnyak, arXiv:1810.11470.
[36] P.-X. Shen, S. Hoffman, and M. Trif, arXiv:1912.11458.
[37] E. Barouch and B. M. McCoy, Phys. Rev. A **3**, 786 (1971).
[38] S. Sachdev, Nucl. Phys. B **464**, 576 (1996).
[39] L. Banchi, P. Giorda, and P. Zanardi, Phys. Rev. E **89**, 022102 (2014).
[40] M. V. Medvedyeva and S. Kehrein, Phys. Rev. B **90**, 205410 (2014).
[41] I. Klich and L. Levitov, Phys. Rev. Lett. **102**, 100502 (2009).
[42] H. F. Song, S. Rachel, and K. Le Hur, Phys. Rev. B **82**, 012405 (2010).
[43] H. F. Song, C. Flindt, S. Rachel, I. Klich, and K. Le Hur, Phys. Rev. B **83**, 161408(R) (2011).
[44] H. F. Song, S. Rachel, C. Flindt, I. Klich, N. Laflorencie, and K. Le Hur, Phys. Rev. B **85**, 035409 (2012).
[45] S. Sachdev, *Quantum Phase Transitions*, 2nd ed. (Cambridge University Press, Cambridge, 2011).
[46] Y. Castin, in *Proceedings of the International School of Physics "Enrico Fermi"*, edited by M. Inguscio, W. Ketterle, and C. Salomon (SIF, Bologna, Italy, 2007), pp. 289–349.
[47] G. Vidal, J. I. Latorre, E. Rico, and A. Kitaev, Phys. Rev. Lett. **90**, 227902 (2003).
[48] A. R. Its and V. E. Korepin, J. Stat. Phys. **137**, 1014 (2009).
[49] P. Calabrese and J. Cardy, J. Stat. Mech. (2004) P06002.
[50] V. Eisler and Z. Zimborás, Phys. Rev. A **89**, 032321 (2014).
[51] P. Ribeiro, Phys. Rev. B **96**, 054302 (2017).